NÖHÜ Müh. Bilim. Derg. / NOHU J. Eng. Sci., 2023; 12(1), 113-118

Niğde Ömer Halisdemir Üniversitesi Mühendislik Bilimleri Dergisi
Niğde Ömer Halisdemir University Journal of Engineering Sciences

Araştırma makalesi / Research article

www.dergipark.org.tr/tr/pub/ngumuh / www.dergipark.org.tr/en/pub/ngumuh

Design and fabrication of compact Wilkinson power divider on gallium nitride coplanar technology

Galyum nitrür koplanar dalga kılavuzu teknolojisinde kompakt Wilkinson güç bölücü tasarımı ve üretimi

Galip Orkun Arıcan[1,*]

[1] *ASELSAN Inc., Communication and Information Technologies Division, 06200, Ankara Türkiye*

Abstract

In this article, an ultra-compact monolithic microwave integrated Wilkinson power divider (WPD) was accomplished for X-band applications. So as to reduce the size of the design, the miniaturization technique was illustrated with the theoretical analysis. After the theoretical analysis, the layout of the design and electromagnetic simulation were performed. The proposed Wilkinson power divider was manufactured with utilizing gallium nitride integrated passive device technology. In the measurement results, it was seen that the input and output (I/O) reflection coefficients were better than -15 dB in the frequency bandwidth of 8-12 GHz. In addition, the transmission coefficient was measured less than -4 dB in the X-band (8-12 GHz). Moreover, the 15-dB fractional bandwidth is 40% and the isolation between the outputs are better than -15 dB. The size of the proposed Wilkinson power was reduced to the dimensions of 700 µm × 700 µm (0.0023 λ_g x 0.0023 λ_g, where λ_g is the wavelength value at the center frequency (10 GHz)), as π-type miniaturization technique was employed with monolithic lumped components. Beside its miniaturized size, the proposed power divider exhibits broadband characteristics while having any degradation in the electrical performance.

Keywords: Wilkinson power divider, Coplanar waveguide, Integrated passive device, Compact

Öz

Bu makalede, ultra-kompakt mikrodalga tektaş Wilkinson güç bölücü entegre devre tasarımı X-bant uygulamaları için gerçekleştirilmiştir. Tasarımın boyutunun küçültebilmesinde minyatürleştirme tekniği kullanılarak, teorik olarak hesaplamaları anlatılmıştır. Teorik analizlerin tamamlanmasından sonra, tasarımın serim tasarımı yapılarak elektromanyetik benzetimleri gerçekleştirilmiştir. Önerilen devre tasarımı, galyum nitrür tümdevre pasif devre teknolojisi kullanılarak üretilmiştir. Ölçüm sonuçlarına göre, giriş ve çıkış (I/O) yansıma katsayılarının 8-12 GHz frekans bandı içerisinde -15 dB'den daha iyi olduğu görülmüştür. Ek olarak, X-bantta (8-12 GHz) araya iletim katsayısının -4 dB'den düşük olarak ölçülmüştür. Ayrıca, elde edilen ölçüm sonuçlarına göre prototipin 15-dB bant genişliği %40 olarak hesaplanmıştır ve çalışma frekans bandı içerisinde çıkış portları arasındaki izolasyonun -15 dB'den daha iyi olduğu görülmüştür. Ayrıca, önerilen Wilkinson güç bölücü tasarımının boyutu, π-tipi minyatürleştirme tekniğinde tümdevre devre elemanları kullanılarak 700 µm × 700 µm (0.0023 λ_g x 0.0023 λ_g, burada λ_g merkez frekanstaki (10 GHz) dalga boyu değeridir) boyutlarına kadar düşürülmüştür. Geliştirilen güç bölücünün ölçüm sonuçlarına göre, minyatür boyutuna rağmen, elektriksel performansında herhangi bir kötüleşme olmadan geniş bantlı bir karakteristik sergilediği görülmüştür.

Anahtar kelimeler: Wilkinson güç bölücü, Koplanar dalga kılavuzu, Pasif entegre aygıt, Kompakt

1 Introduction

Power dividers, that are widely utilized with great RF characteristics, are in high demand with the day by day improvements in modern communication systems, such as amplifiers, mixer, power sensors, phase detectors, antennas and many other applications [1, 2]. The Wilkinson power divider (WPD) is utilized to divide the received signal into two outputs with equal both phase and amplitude. WPD has the characteristic of having low insertion loss, high isolation and good matching [3]. In addition, the conventional WPD has a simple structure that can be constructed with two quarter wavelength (λ/4) transmission lines and an isolation resistor between the output ports [4]. Besides these advantages, the conventional WPD can be notably large in size with the narrow frequency bandwidth in the lower frequency spectrum, especially below Ku-band. Due to this reason, development of the broadband miniaturized WPD has become a challenging topic, especially for low-cost and size-constrained system manufacture. In the literature, the inductive/capacitive loaded lumped elements, T- and π-type equivalent circuits, open circuit stubs, resonators, tapered transmission lines, high impedance and step impedance multilayer structures have been investigated for microstrip technology to overcome miniaturization issues [5-12]. In addition, these miniaturization techniques have been applied with utilizing multi-layer printed circuit board, low temperature co-fired ceramics (LTCC), III-V semiconductor

* Sorumlu yazar / Corresponding author, e-posta / e-mail: goarican@aselsan.com.tr (G.O. Arıcan)
Geliş / Recieved: 29.07.2022 Kabul / Accepted: 17.11.2022 Yayımlanma / Published: 15.01.2023
doi: 10.28948/ngumuh.1151080

integrated passive device (IPD) process [13-14]. Nevertheless, the WPD with coplanar waveguide (CPW) technology becomes a notable choice to microstrip WPD by dint of having low manufacturing complexity, no via holes and low-loss [15]. Moreover, broadband and low-dispersion characteristics can be accomplished with utilizing CPW rather than the microstrip technology [12]. Thus, CPW technology picks a great interest to enhance a low-cost compact WPD in behalf of the simple integration the electronic systems. On the other hand, wide-bandgap semiconductors, such as aluminium nitride (AlN), silicon carbide (SiC), gallium nitride (GaN), silica (SiO2) and boron nitride (BN), become promising alloys for modern communication systems [16-17]. Furthermore, GaN is a glaring alloy for solid-state devices with high-speed data transmission, high-power handling capability and high thermal conductivity characteristics.

In this study, an ultra-compact coplanar-waveguide Wilkinson power divider was developed with utilizing gallium nitride integrated passive device manufacturing process for modern communication systems. In the proposed WPD, the lumped elements and π-type miniaturization technique was utilized to replace the λ/4 transmission lines with the spiral inductor between the shunt capacitors. The proposed miniaturization technique was analyzed theoretically and the theoretical results were verified with both electromagnetic (EM) simulations and on-wafer measurement. The proposed divider has a very compact size of 700 µm × 700 µm and it yields an 88% size reduction and covers all of the X-band (8-12 GHz).

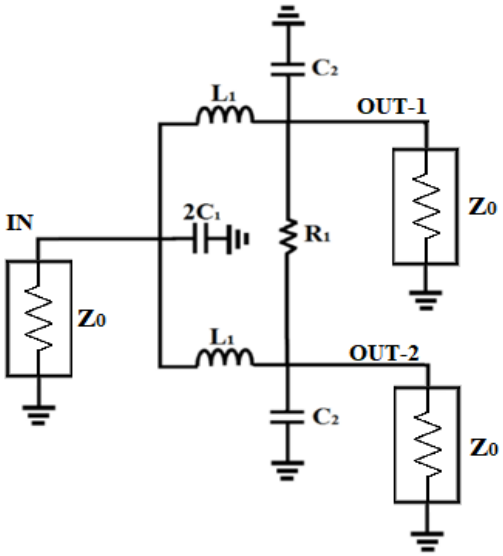

Figure 1. Equivalent circuit model of the proposed WPD

2 Material and method

2.1 Overview of the WPD

A conventional WPD is a symmetrical circuit that consists of two λ/4 transmission lines with the characteristic impedance of $\sqrt{2}Z_0$ where Z_0 is the characteristic impedance [4]. So as to enhance the isolation between the output ports, an isolation resistor of $2Z_0$ was utilized between the outputs [4]. The WPD splits the instant signal into two output signals with equal phase and amplitude. However, the λ/4 transmission line consumes too much costly chip area in the low-end frequency spectrum. In order to minimize the occupied chip size, the lumped elements and miniaturization techniques needs to be applied. In the proposed WPD, λ/4 transmission lines were realized with π-type equivalent network that was established with the lumped components of spiral inductor between the metal insulator metal (MIM) capacitors. Figure 1 depicts the equivalent circuit model of the proposed WPD.

2.2 Design and analysis of the proposed WPD

In the proposed design, the π-type equivalent network topology with the lumped monolithic microwave components were utilized instead of λ/4 transmission line. In addition, the π-type equivalent network was constructed with utilizing a spiral inductor between the shunt capacitors. The values of the lumped components were calculated theoretically with utilizing [ABCD] parameters. Figure 2 depicts the equivalent circuit model of the transmission line.

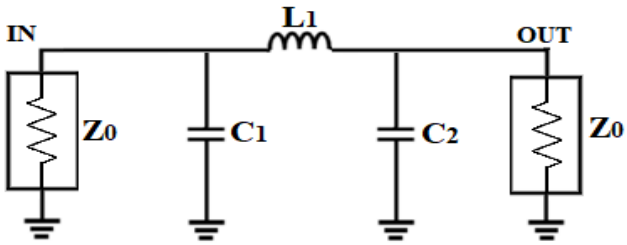

Figure 2. Equivalent circuit model of the transmission line

The [ABCD] parameters of the equivalent circuit model of the transmission line (M_E) can be expressed as the multiplication of the [ABCD] parameters of the lumped components.

$$M_E = M_{C1} M_{L1} M_{C2} \tag{1}$$

where M_{C1} is the shunt capacitor (C_1), M_{L1} is the series inductor (L_1) and the M_{C2} is the shunt capacitor (C_2). If the [ABCD] parameters of the lumped components are added in to the equation 1, the M_E can be expressed as given in the Equation (2).

$$\begin{bmatrix} A & B \\ C & D \end{bmatrix} = \begin{bmatrix} 1 & 0 \\ jB_1 & 1 \end{bmatrix} \begin{bmatrix} 1 & jX_L \\ 0 & 1 \end{bmatrix} \begin{bmatrix} 1 & 0 \\ jB_2 & 1 \end{bmatrix} = \begin{bmatrix} 1 - jX_L B_2 & jX_L \\ j(B_1 + B_2) - jX_L B_1 B_2 & 1 - X_L B_1 \end{bmatrix} \tag{2}$$

where $B_1=\omega C_1$; $B_2=\omega C_2$ and $X_L=\omega L_1$. In addition, the transmission line (MTL) can be extended in the [ABCD] matrix as in the Equation (3).

$$M_{TL} = \begin{bmatrix} \cos\beta l & jZ_c \sin\beta l \\ jY_c \sin\beta l & \cos\beta l \end{bmatrix} \tag{3}$$

In the Equation (3), Z_C and l denote the characteristic impedance and electrical length of the transmission line, respectively.

$$Z_C = \sqrt{2}Z_0 \tag{4}$$

$$\beta l = \frac{2\pi}{\lambda}\frac{\lambda}{4} = \frac{\pi}{2} \tag{5}$$

If the matrices of M_E and M_{TL} are equal to each other and the Equations (4) and (5) are put into the Equation (3), the matrix can be solved as Equations (6-8):

$$C_1 = \frac{1}{\omega Z_c} \tag{6}$$

$$C_2 = \frac{1}{\omega Z_c} \tag{7}$$

$$L_1 = \frac{Z_c}{\omega} \tag{8}$$

$$R_1 = 2Z_0 \tag{9}$$

In the theoretical analysis of the equivalent circuit design, the lumped components can be calculated as C_1 and C_2 are 225 fF, L_1 is 1125 pH and R_1 is 100 Ω for the center frequency of 10 GHz.

3 Results and discussion

The layout of the proposed WPD was designed in the Advanced Design System (ADS) Momentum software which is a planar electromagnetic simulator. In addition, ADS Momentum employs method of moments (MoM) to solve the numerical electromagnetic field analysis. In the layout design, the inductors were realized with the spiral inductors and the capacitors were realized with MIM capacitor. Moreover, the input and output terminal were designed to be able to do on-wafer measurements. Hence, the ground planes were connected with each other utilizing underpass metallization and the signal cross over the underpass metal with air bridge structures. Furthermore, the isolation resistor was realized with NiCr metallization. The total dimension of the proposed WPD including RF pads are 700 µm x 700 µm which is 0.0023 λ_g x 0.0023 λ_g, where λ_g is the wavelength value at the center frequency (10 GHz). Figure 3 depicts the layout of the proposed WPD and the dimensions of the proposed WPD is given in the Table 1.

Figure 4 depicts the current density distribution of the proposed WPD at 10 GHz. The current density distribution shows that the current density increases especially on the underpass metals inside the spiral inductors and on the air bridge structures.

The prototype of the proposed WPD was manufactured with utilizing Gallium Nitride (GaN) on Silicon Carbide (SiC) integrated passive device (IPD) process in Nanotechnology Research Center. GaN IPD process was preferred to manufacture the proposed WPD because of having high power handling capability and high thermal conductivity. These advantages give GaN MMIC process to be utilized both in the high-frequency and high-power applications. In addition, GaN epitaxial layer was grown on a 300 µm SiC substrate with a dielectric constant of 9.8 at 300°K. Nickel Chrome (NiCr) resistor, which has 30 Ω/square sheet resistance (R_s), was realized with utilizing e-beam evaporating process. Moreover, the GaN IPD process has a contact resistance of a typically 0.25 Ω.mm in the transmission line measurement (TLM). In addition, GaN IPD process possess two (Au) metallization layers which are metal-1 and metal-2 with the thickness of 1 µm and 3 µm, respectively. Furthermore, metal insulator metal (MIM) capacitor is realized with utilizing a Silicon Nitride (Si_3N_4) passivation layer with 0.3 µm thickness between the two metal layers. The passivation layer has a dielectric constant of 6.8. Nevertheless, the air bridge structure is utilized for metal-2 layer to cross the metal-1 and NiCr resistor layers on the substrate. Figure 5 depicts the cross-section of the GaN CPW IPD technology.

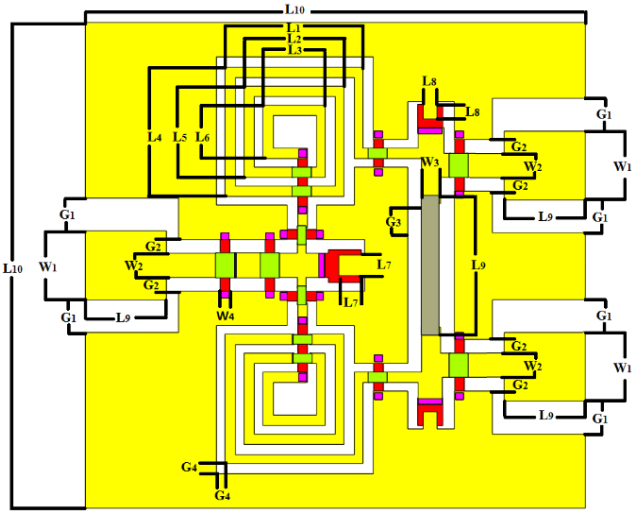

Figure 3. Layout of the proposed WPD (700 µm x 700 µm)

Table 1. The dimensions of the layout

Parameter	Value (µm)	Parameter	Value (µm)
L1	204	L6	78
L2	148	L7	32
L3	92	L8	16
L4	190	L9	206
L5	134	L10	700
W1	100	G1	52
W2	37	G2	19
W3	26	G3	23
W4	14	G4	14

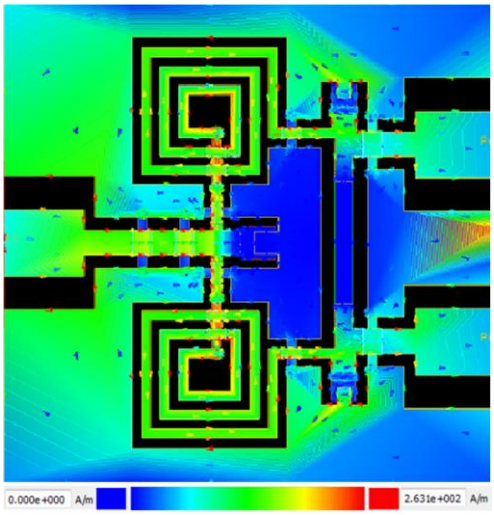

Figure 4. The current density of the proposed WPD (10 GHz)

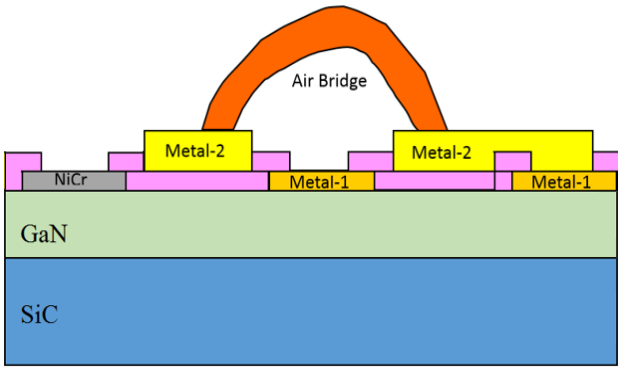

Figure 5. Cross-section of the GaN CPW IPD technology

The Agilent E8361C network analyzer, Cascade RF1 microwave probe station and GGB 40A-GS-150-P RF probes were utilized in the on-wafer prototype measurements. Before the on-wafer measurements, the short open load thru (SOLT) calibration was applied at the reference points. According to the bandwidth percentage Equation (10), the bandwidth was calculated as 40% for 15-dB I/O reflection coefficient. Moreover, f_0 denotes the center frequency and the f_1 and f_2 denotes the lower and upper frequency band, respectively. Furthermore, the frequency ration was calculated as 6, according to the Equation (11).

$$BW\% = \frac{f_2 - f_1}{f_0} \tag{10}$$

$$\kappa = \frac{f_2}{f_1} \tag{11}$$

The prototype was manufactured to verify the accuracy of the design with utilizing GaN CPW IPD technology. Figure 6 depicts the photography of the prototyped WPD.

In the S-parameter measurement, the input reflection coefficient (S_{11}) was lower than -15 dB, in the operating frequency bandwidth of 8-12 GHz. Figure 7 depicts the simulated and measured reflection coefficient (S_{11}) of the proposed WPD.

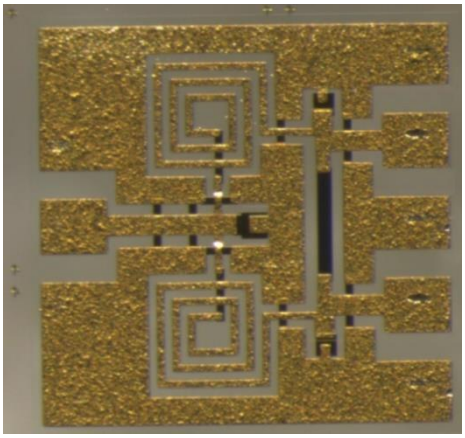

Figure 6. The photography of the prototyped WPD

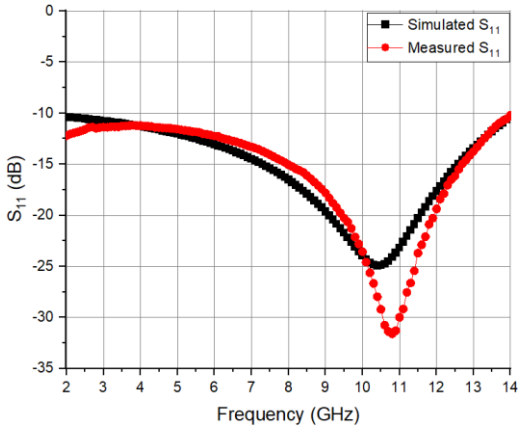

Figure 7. The simulated and measured S_{11} of the proposed WPD

In addition, the output reflection coefficients (S_{22} & S_{33}) were measured lower than -15 dB in the frequency bandwidth of 8-12 GHz. Figure 8 depicts the output reflection coefficients (S_{22} & S_{33}) of the proposed WPD.

Moreover, the transmission coefficient (S_{21}) was measured less than -4 dB in the frequency bandwidth of 8-12 GHz. Figure 9 depicts the simulated and measured transmission coefficients (S_{21} & S_{31}) of the proposed WPD.

The measured isolation was less than -15 dB in the operating frequency bandwidth of 8-12 GHz. Figure 10 depicts the simulated and measured isolation (S_{23}) between the outputs of the proposed WPD.

The phase inequality between the outputs was less than 1.1° the frequency bandwidths of 8-12 GHz. The simulated and measured phase inequality of the outputs were in good agreement with each other. The measured phase difference between the output ports was better than the simulation result in the frequency bandwidth of 3.5-10.5 GHz and lowest phase difference between the outputs was achieved at around 6 GHz. Moreover, the highest variation between measured and simulated phase difference was observed at around 6 GHz with phase difference of ~0.7°. On the other hand, the variation between the measurement and simulation results

was occurred in a similar increasing trend with phase difference of ~0.1° at frequencies higher than 11 GHz. The slight difference between the measurement and simulation results would be caused by the manufacturing tolerances. Figure 11 depicts the simulated and measured phase inequality between the outputs of the proposed WPD.

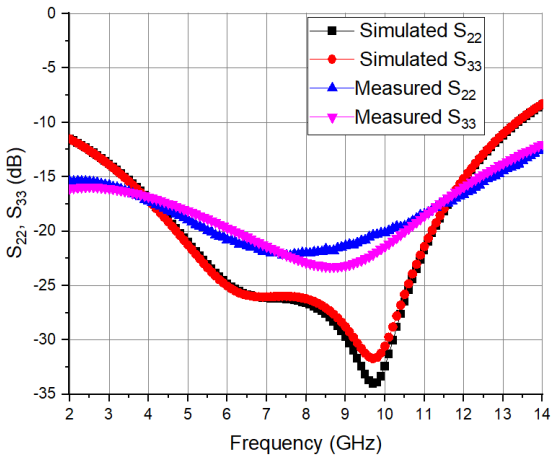

Figure 8. The simulated and measured S_{22} and S_{33} of the proposed WPD

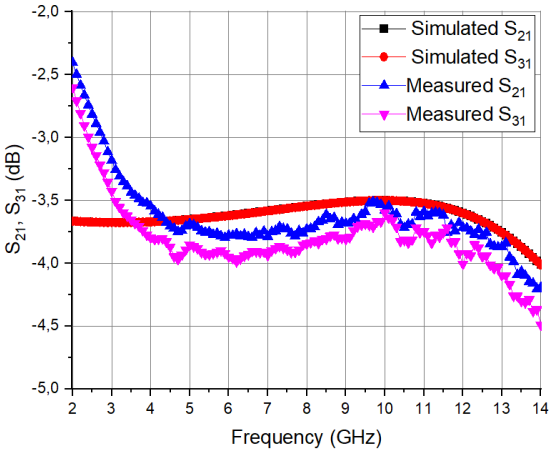

Figure 9. The simulated and measured S_{21} and S_{31} of the proposed WPD

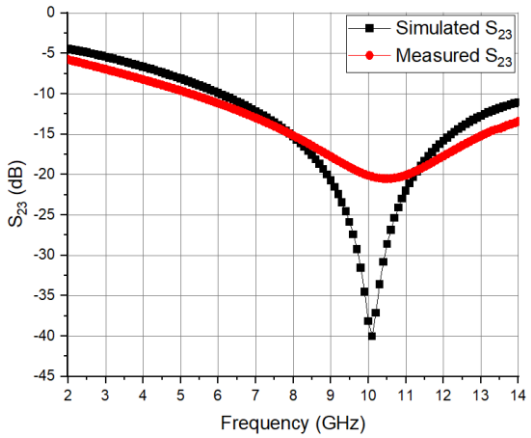

Figure 10. The simulated and measured isolation S_{23} between the outputs of the proposed WPD

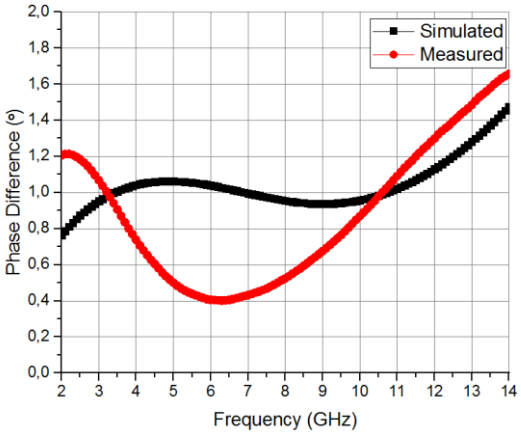

Figure 11. The simulated and measured phase inequality between the outputs

4 Conclusions

In this letter, an ultra-compact WPD was presented, which was developed by utilizing lumped components with coplanar waveguide integrated passive device process in the gallium nitride technology. In the proposed WPD design, the π-type miniaturization technique with lumped component was utilized to reduce the chip area. The arms of the proposed WPD, were constructed with MIM capacitors and spiral inductors. The proposed WPD has a total size of 700 µm x 700 µm which yields a size reduction of 88% with respect to the conventional WPD and the fractional bandwidth achieves 40%. The theoretical and experimental results were compatible with each other and the results show that the WPD can be significantly reduced with the miniaturization techniques without any electrical performance degradation. The measurement results show that the prototyped WPD has I/O reflection coefficients better than -15 dB with a transmission coefficient of -4 dB in the frequency range of 8-12 GHz. The proposed WPD can easily be integrated into the monolithic microwave integrated circuits and hybrid modules with its simple and low-cost structure for X-band applications.

Conflict of interest

The author declares that there is no conflict of interest.

Similarity rate (iThenticate): 15%

References

[1] Y. Wang, X. Y. Zhang, F. X. Liu and J. C. Lee, A compact bandpass Wilkinson power divider with ultra-wide band harmonic suppression. IEEE Microwave and Wireless Components Letters, 27(10), 888-890, 2017. https://doi.org/10.1109/LMWC.2017.2745484.

[2] F. Khajeh-Khalili, M. A. Honarvar, A. Dadgarpour, B. S. Virdee and T. A. Denidni, Compact tri-band Wilkinson power divider based on metamaterial structure for Bluetooth, WiMAX, and WLAN applications. Journal of electromagnetic waves and applications, 33(6), 707-721, 2019. https://doi.org/10.1080/09205071.2019.1575287.

[3] A. M. Darwish, A. A. Ibrahim, J. X. Qiu, E. Viveiros, and H. Hung, A Broadband 1-to-n power divider/combiner with isolation and reflection cancellation. IEEE Transactions on Microwave Theory and Techniques, 63(7), 2253-2263, 2015. https://doi.org/10.1109/TMTT.2015.2431690.

[4] D. M. Pozar, Microwave engineering. Wiley, New York (NY), 2012.

[5] P. Rostami and S. Roshanı, A miniaturized dual band Wilkinson power divider using capacitor loaded transmission lines. AEU-International Journal of Electronics and Communications, 90, 63-68, 2018. https://doi.org/10.1016/j.aeue.2018.04.014.

[6] C. H. Tseng and C. H. Wu, Compact planar Wilkinson power divider using π-equivalent shunt-stub-based artificial transmission lines. Electronics Letters, 46(19), 1327-1328, 2010. https://doi.org/10.1049/el.2010.2194.

[7] S. Kaijun, Extremely compact ultra-wideband power divider using hybrid slotline/microstrip-line transition. Electron Letters, 51(24), 2014-2015, 2015. https://doi.org/10.1049/el.2015.2924.

[8] C. L. Chang and C. H. Tseng, Compact Wilkinson power divider using two-section asymmetrical T-structures. Electron Letters, 49, 546–547, 2013. https://doi.org/10.1049/el.2013.0366.

[9] Z. X. Du, X. Y. Zhang, K. X., Wang, H. L. Kao, X. L. Zhao and X. H. Li, Unequal Wilkinson power divider with reduced arm length for size miniaturization. IEEE Transactions on Components, Packaging and Manufacturing Technology, 6(2), 282-289, 2016. https://doi.org/10.1109/TCPMT.2015.2513763.

[10] R. Mirzavand, M. M. Honari, A. Abdipour, and G. Moradi, Compact microstrip Wilkinson power dividers with harmonic suppression and arbitrary power division ratios. IEEE Transaction Microwave Theory Techniques, 61, 61–68, 2013. https://doi.org/10.1109/TMTT.2012.2226054.

[11] Z. Guo and Y. Yang, A novel compact Wilkinson power divider with controllable harmonic suppression and simple structure. Journal of Electromagnetic Waves and Applications, 32(5), 601–608, 2018. https://doi.org/10.1080/09205071.2017.1400926.

[12] Q. Li, Y. Zhang and C. T. M. Wu, High-selectivity and miniaturized filtering Wilkinson power dividers integrated with multimode resonators. IEEE Transaction of Components Packaging and Manu facturing Technology, 7, 1990–1997, 2017. https://doi.org/10.1109/TCPMT.2017.2706958.

[13] J. Han and X. Liao, Miniaturization of a broadband power divider for X-band application based on GaAs technology. Microwave Optical Technologies Letter, 59(6), 1427-1431, 2017. https://doi.org/10.1002/mop.30557.

[14] Y. Jiang, K. Hu, L. Feng, H. Zhang, Y. Shi, W. Tang, and X. Yu, Ultra wideband lumped Wilkinson power divider on gallium arsenide integrated passive device technology. International Journal of RF and Microwave Computer-Aided Engineering, 31(12): e22898, 2021.https://doi.org/10.1002/mmce.22898.

[15] T. Okan, A Wideband conductor backed coplanar waveguide fed ımplantable antenna operable in different tissues for biotelemetry applications. Radioengineering, 30(2), 335-431, 2021. https://doi.org/10.13164/re.2021.0335.

[16] J. V. Gaitonde and R. B. Lohani, Analysis of wide-bandgap material OPFET UV detectors for high dynamic range imaging and communication applications. Communications and Network, 11(4): 83-117, 2019. https://doi.org/10.4236/cn.2019.114007.

[17] M. P. Mikhailova, K. D. Moiseev and Y. P. Yakovlev, Discovery of III–V semiconductors: physical properties and application. Semiconductors, 53(3), 273-290, 2019. https://doi.org/10.1134/S1063782619030126